Low Energy Sputter Yields for Diamond, Carbon-Carbon Composite, and Molybdenum Subject to Xenon Ion Bombardment

J. J. Blandino and D. G. Goodwin
Division of Engineering and Applied Science
California Institute of Technology
Pasadena California 91125

C. E. Garner
Jet Propulsion Laboratory
California Institute of Technology
Pasadena California 91109

Abstract

Sputter yields have been measured for polycrystalline diamond, single crystal diamond, a carbon-carbon composite, and molybdenum subject to bombardment with xenon. The tests were performed using a 3 cm Kaufman ion source to produce incident ions with energy in the range of 150 – 750 eV and profilometry based technique to measure the amount of sputtered material. The yields increased monotonically with energy with values ranging from 0.13 at 150 eV to 0.70 at 750 eV for the molybdenum and 0.05 to 0.13 for the carbon-carbon. At 150 and 750 eV the yield for both diamond samples was 0.05 and 0.16, respectively within the experimental uncertainty. A number of experimental factors affecting sputter yield measurements using this technique are described.

Introduction

In recent years there has been significant progress made in the production of chemically vapor deposited (CVD) diamond films. Improvements in quality, reproducibility, and growth rates (> 10 μm hr^{-1}) have made diamond films attractive for a variety of applications in the fields of electronics, optics, and tribology among others[1,2,3]. One potential application under evaluation at the Jet Propulsion Laboratory involves the use of diamond films as coatings for ion thruster electrodes which are subject to sputter erosion[4]. A number of studies have examined the sputtering characteristics of both single crystal and polycrystalline diamond at incident ion energies less than 2.0 keV. Most of these have used argon[5-10] as the incident ion species with some work also evaluating neon[9,11] and oxygen.[5,7,12,13,14] One study considering the role of nitrogen in the reactive etching of diamond also used 2 keV xenon ions[15]. Different experimental approaches used to quantify removed material have included profilometry to measure eroded depth profiles as well as direct mass loss measurements. A variety of ion sources have also been used including immersion of a self biased target into an RF plasma, and externally accelerated ion beams using Kaufman and ECR sources. While most of these studies involved exposure of the samples to energetic ions at normal incidence, a systematic evaluation of the incidence angle dependence of the yield of the (100) face of single crystal diamond subject to argon ion bombardment has also been reported[5]. In the present paper, results for the sputter yield and corresponding erosion rate of diamond

subject to xenon ion bombardment at energies of 150, 250, 500, and 750 eV are presented. The yield and erosion rate for molybdenum and carbon-carbon composite, both in use as electrode materials for ion thrusters, were also determined.

Experiment

The experimental approach used to measure the sputter yields in this work consisted of exposing selectively masked areas of the different samples to an ion beam for a prescribed period of time. The depth of the resulting eroded valley can then be measured to calculate the number of atoms removed. A probe located adjacent to the samples records the beam current density which can then be integrated to determine the incident ion dose. During exposure of the samples it is important to minimize the influence of residual facility gases. Previous work suggests that the presence of nitrogen can lower the erosion rate of metals[16] whereas oxygen in the presence of energetic ions can reactively etch diamond.[13,14] Reactive ion etching is one technique which has been used successfully to etch structures in diamond. Efremow et al. used a NO_2 gas jet incident on a diamond surface while the target was under bombardment with 2 keV xenon ions[15]. The incident ions in this case provide the activation energy required to form CO and CO_2 volatiles. Minimizing contamination is therefore essential to reduce the chance of reactively eroding the carbon targets and obtaining artificially high sputter yields. For these reasons the present test was conducted in a facility capable of low ultimate pressures ($< 10^{-9}$ Torr).

The system used was an ultra-high-vacuum chamber with a 3 cm Kaufman ion source (Commonwealth Scientific Corp.) normally used for sputter deposition. The vacuum chamber geometry is depicted in Figure 2. The system is pumped with a turbomolecular pump (115 l/sec) backed by a small mechanical pump (0.8 l/sec) down into the 10^{-4} Pa (10^{-6} Torr) range and then with a 6" cryopump (1500 l/sec) to the 10^{-7} Pa (10^{-9} Torr) range. The base and test pressures for each of the cases are summarized in Table 1. As an additional measure, the chamber was baked at over 100 C every evening for several hours.

One drawback of using a chamber measuring approximately 12 inches high by 15 inches wide is the relative inflexibility of sample and probe placement. The samples were located approximately 6.7 cm downstream of the source exit plane. Although proximity of the targets to the ion source increases the incident current density and shortens the required exposure time, it also results in non-uniformity of the ion current profile over the samples which then has to be accounted for.

The experimental approach included centering the probe on the point of maximum current density in the beam which was subject to some drift over the duration of each test. This was accomplished through a combination of vertical translation, and rotation of the sample platform (see Figure 2). Both of these motions, in addition to the divergence of the beam, will affect the incidence angle of the incoming ions. Table 1 lists the calculated incidence angles 1 for the four tests assuming the beam originates at the center of the source exit plane and terminates at the center point of the probe. Because

the probe position is adjusted slightly at various times throughout the test to insure it is located at the point of maximum beam current, the incidence angles reported in Table 1 have been time averaged over the duration of each test.

The samples used in the test were mounted on a fixture and covered with a Tantalum foil mask. After the exposed area of the samples had been eroded, the depth of the eroded valley in the target material was measured with a profilometer. The CVD diamond sample used was commercially produced in a DC arcjet CVD process and polished (on one side) to a mirror finish. Details of its production including the gas mixture, growth temperature, the substrate used and the polishing technique employed are proprietary to Crystalline Materials Corp. Only one sample was available for these measurements so the chip, which was approximately 1 cm on a side was rotated between tests to expose different areas. Two of the tests were performed on the unpolished side of the chip as discussed later. The single crystal diamond samples were (110) oriented except for the one used in the 500 eV test which was (100). These diamond samples were 2 mm diameter, 0.25 mm thick disks produced commercially in the Netherlands.

Analysis

Number of Sputtered Target Atoms

One assumption inherent in using a profilometer to estimate the number of atoms removed from the target is that the valley depth represents an averaged volume removed per unit area where in fact it only represents the eroded profile at the location where the trace is taken. A true average would require multiple profilometer scans and then an integration of the "slices" to calculate the eroded volume. The diagram in Figure 1 illustrates the relevant dimensions used in the calculation of eroded depth. Measuring the depth only at the center of the valley does not adequately take into account the profile of the valley walls which may not be vertical. It was found that the molybdenum tended to have more vertical walls than the polycrystalline diamond in which the valley walls sloped gently. In order to calculate a sputtered volume per unit area, or mean effective depth, the depth profile was integrated according to

$$h_{eff} = \frac{1}{(x_r - x_l)} \int_{x_l}^{x_r} (y(x)_{mean} - y(x)_{valley}) dx \qquad (1)$$

The traces obtained from the profilometer were scanned into a computer and digitized. In addition to facilitating the integration in Equation 1, this digitized mesa-valley-mesa profile could be subjected to statistical analysis to quantify surface roughness.

A least squares line fit through the mesa points establishes a datum, $y(x)_{mean}$, from which the valley depth at each x location can be measured. There is a standard deviation associated with this line fit as a result of the mesa surface roughness which is incorporated into the overall uncertainty estimate. The effective depth h_{eff} is then used to calculate the number N_A of target atoms removed per unit area;

$$N_A = \rho h_{eff} \frac{N_{avo}}{M} \quad (2)$$

where N_{avo} is Avogadro's number, M the molecular weight, and ρ the target density. The values for the sample density used in calculating the yields were 10.2 g/cm^3 for molybdenum, 1.65 g/cm^3 for carbon-carbon, and 3.5 g/cm^3 for the CVD diamond. The diamond sample was a square roughly 1 cm on a side and less than a millimeter thick. It had a chip and some cracks which made a volume estimate difficult to obtain accurately. For this reason the density was estimated to be that of single crystal diamond. SEM imaging of the sample did not reveal any evidence of porosity suggesting this assumption is valid within the experimental uncertainty.

Incident Dose of Energetic Particles

The ion current incident on the target was measured and recorded throughout the test by a planar probe. This probe surface was a 0.063 inch diameter tungsten disk which was biased to 25 V below facility ground to insure operation in the ion saturation regime. There are several factors which affect the incident ion dosage estimate and contribute to the experimental uncertainty in the reported measurements. These include secondary electron emission from the probe, thermal charge-exchange ions and energetic neutrals incident on the probe, collection of doubly ionized gas atoms, and non-uniformity of the beam current density. Each of these will be discussed in the following paragraphs.

Secondary Electron Emission

Because a secondary electron emitted from a current probe is indistinguishable from an arriving ion, operation either at high energies or with probe materials with a high secondary electron emission coefficient require a correction. In this work, the measured current was corrected for secondary electron emission using data from Reference 17. For a tungsten probe with ion energies below 1 keV, this correction is small (< 1.5 percent).

Thermal Charge-Exchange Ions and Energetic Neutrals

Charge exchange (CEX) collisions occur when a fast ion exchanges an electron with a thermal neutral producing a thermal ion and a fast neutral. These collisions can occur between atoms of the same species (symmetric resonant collisions) or between atoms of different species (asymmetric nonresonant collisions)[18]. Fast neutrals will sputter the target but not be accounted for in the current measurements while thermal ions may be collected by the current probe but are likely to be below the sputter energy threshold of most target materials. Whether the contribution of CEX ions is relevant for a particular experiment depends in large part on the type of ion source used. When a self biased sample is placed in an RF plasma for instance, the ions will gain their energy as they accelerate through the sheath. Because the sheath thickness is likely to be small relative to the mean free path for CEX

collisions it is unlikely a significant population of energetic neutrals could be produced. For a Kaufman source the energetic ions travel through several centimeters of neutral gas before reaching the target.

Because the base pressure for these tests was relatively low, the dominant source of gas atoms which are available to become charge exchange ions will be the unionized xenon from the discharge chamber, a fraction of which will drift out through the grids and into the beam. The ratio of the beam current to the total gas mass flow rate (expressed as a current) is defined as the gas utilization efficiency. For commercial ion sources used primarily for sputter deposition (as opposed to propulsion), this efficiency can be quite low resulting in significant loss of unionized gas through the grids. For each of the four cases presented here, this efficiency was less than ten percent. For this reason, a correction must be made to avoid over (or under) estimating the dosage of energetic sputtering ions (or atoms). The total current collected at the probe is given by

$$J_p = J_b(1+\gamma_2) + J_{cex} + \gamma_2 J_n$$

where J_b is the energetic beam current, γ_2 the secondary electron emission coefficient, J_{cex} is the charge-exchange ion current incident on the target (i.e. the flux of thermal CEX ions) and $\gamma_2 J_n$ is the current registered as a result of secondary electrons emitted when an energetic neutral atom arrives at the probe. In this last term, the flux of energetic neutral atoms has been expressed as an equivalent current (i.e. $J_n = e\Gamma_n A_{probe}$). Because one is really interested in dosages, the currents are integrated over the duration of the exposure τ to obtain an expression for the total delivered charge Q_b due to beam ions.

$$Q_b = \frac{1}{1+\gamma_2}\left[\int_0^\tau J_p(t)dt - \int_0^\tau J_{cex}(t)dt - \int_0^\tau \gamma_2 J_n(t)dt\right] \qquad (3)$$

The first integral in the brackets represents the uncorrected, recorded probe current. This was integrated graphically from the strip chart data for the probe. The second and third integrals represents the dosages of charge-exchange ions collected and secondary electrons emitted from the probe as a result of energetic neutral bombardment. The last two terms in Equation 3 are generally not known as functions of time. Reference 18 presents a methodology for estimating the beam current reaching the target as a function of the charge-exchange collision cross section and background neutral gas pressure. Because of low scattering angles, the energetic neutrals produced in these collisions are assumed to continue in their original direction with the same energy.[18]

To estimate the last two integrals in Equation 3, a pair of differential equations were derived in a manner similar to that employed in Reference 18 for the beam ions. These two equations described the conservation of both beam ions and CEX ions in a divergent beam with a prescribed neutral background density distribution. The background neutral density function included a decaying term representing gas drifting through the source accelerator grid as well as a constant term representing the ambient background gas pressure in the chamber. This representation of the neutral density distribution followed one used in Reference 19 for the numerical modeling of ion thruster plumes. In the one

dimensional model developed for this work, beam ions are converted to charge-exchange ions which are assumed to be Maxwellian at a temperature representative of gas in the chamber. These ions drift isotropically at the thermal velocity and can therefore escape the beam radially. As previously mentioned, the energetic neutrals resulting from CEX collisions are assumed to preserve their original direction. Therefore upon solving for the centerline beam ion flux, the fast neutral flux at the target position can be calculated as well by requiring that directed energetic particles be conserved. The 1-D model was used to estimate the ratio of CEX ion and energetic neutral flux to beam ion flux for the four different test conditions considered. These ratios were then used to evaluate the last two terms in Equation 3.

Doubly Ionized Incident Atoms

Because the probe will count the arrival of a double ion as two single ions, it is necessary to calculate the equivalent single ion dosage at the target. In terms of the double to single ion current ratio

$$R_d = \frac{J_b^{++}}{J_b^{+}}$$

the dosage of single and double ions can be expressed as

$$Q_b^{+} = \frac{1}{1+R_d} Q_b \qquad Q_b^{++} = \frac{R_d}{1+R_d} Q_b$$

Note that the correction for double ion content is applied to the total beam dosage which has already been corrected for the charge exchange ion current. The total dosage of energetic, sputtering ions and energetic neutrals at the target is then

$$N_E = \frac{1}{e}\left(Q_b^{+} + \frac{1}{2} Q_b^{++} + \int_0^{\tau} J_n(t)dt \right) \tag{4}$$

The yield is then given by the ratio of atoms removed to incident energetic particles;

$$Y = \frac{N_A}{N_E} \tag{5}$$

which can be expressed in terms of the previous expressions as

$$Y = \frac{h_{eff}}{\int_0^{\tau} \left(J_p(t) - J_{cex}(t) - \gamma_2 J_n + \frac{1+R_d}{\left(1+\frac{R_d}{2}\right)}(1+\gamma_2) J_n(t)\right) dt} \left[\frac{\rho e N_{avo}(1+\gamma_2)(1+R_d)}{M(1+\frac{R_d}{2})} \right] \tag{6}$$

Although the yield given by Equation 6 is corrected for double ion dosage in terms of the *number* of incident ions, it does not correct for *damage* caused by the double ions which impact with twice the energy. This is a much more difficult correction to make since one would have to have some knowledge of the yield as a function of energy which is what is being calculated. In the present investigation, because of the low gas utilization efficiency (< 10 percent), the neutral density is too high to support any significant number of doubly ionized atoms and the fraction of double ions can be assumed negligible. Setting $R_d = 0$ in Equation 6 results in the following simplified expression for the yield;

$$Y = \frac{h_{eff}}{\int_0^{\tau} (J_p(t) - J_{cex}(t) + J_n(t))dt} \left[\frac{\rho e N_{avo}(1+\gamma_2)}{M} \right] \tag{7}$$

Beam Nonuniformity

In these experiments the probe (and target) was located only 6.7 cm (2.64 in) from the source. With the target and source in such proximity, a potentially significant uncertainty in the measured current is introduced by non uniformity of the beam profile. During the experiment, the probe is centered on the point of maximum current in the beam. This was checked at various times during the experiment by moving the probe slightly and observing the probe current. The eroded portions of the samples are located within a 1.27 cm (0.5 inch) diameter circle centered on the probe. Non-uniformity of the beam results in the current density decreasing away from the probe. Over time, the non-uniformity worsened as a result of localized erosion of the ion source accelerator grid. The resulting perturbation in the beam symmetry was noticeable in a subsequent mapping of the current profile. To correct the dose calculation for beam non uniformity, the density profile maps were used to estimate the incident current at the location of the exposed sample as a fraction of the maximum beam current.

Results

The yield measured for molybdenum is presented in Figure 3 along with data from Rosenberg and Wehner[20] and Weijsenfeld et al.[21]. Both of these previous studies used biased targets placed in plasma sources to provide the incident ions and utilized measurement of target mass loss to determine the quantity of sputtered material.

One significant difference between the present work and these earlier experiments is that in the present work the targets were bombarded at non-normal incidence. In a study of the effect of incidence angle on sputter yields, Wehner[22] determined that metals generally fall into one of three classes; those exhibiting a 1) "very slight angle effect" , 2) "moderate angle effect", and 3) "very pronounced effect". The third group includes iron, tantalum, and molybdenum. For incidence angles relevant to the present work (i.e. less than 30 degrees), the sputter yield increases relative to the value at normal incidence. The fact the yields measured here are lower than these previously reported values suggests that it is

more likely the neutral flux has been overestimated in Equation 7 resulting in an underestimation of the yield.

The absolute yield data for the diamond and carbon-carbon are presented in Figure 4. The carbon-carbon yield shown in Figure 4a increases monotonically with energy, as expected from previous investigations with graphite[20] . Unlike graphite, the carbon-carbon composite consists of graphitic fibers woven together in a carbonaceous matrix, which is in part graphitic and part glassy carbon[23]. Although these targets were polished before testing, examination of the profilometer traces reveal an increase in surface roughness for the carbon-carbon after exposure to the beam, probably resulting from local variation in yield between the fibers and the matrix.

The sputter yield of the polycrystalline diamond is shown in Figure 4b. Any difference in the yield at 150 and 250 eV lies within the experimental uncertainty. As was described in the experiment description section , both sides of the CVD diamond sample were used in the tests. SEM imaging in the eroded valleys corresponding to each of the tests reveal a larger density of pits in the surface used for the 150 and 250 eV tests which were on the opposite (unpolished) side of the same sample used for the 500 and 750 eV tests. It is possible these are areas where the crystallites had not completely covered the substrate during the growth process. In particular, the valley corresponding to the test at 250 eV is seen to be noticeably rougher with a higher surface density of pits. In general the yields for rougher surfaces tend to be lower due in part to re-deposition of sputtered material along sides of surface features. The effect may have resulted in a lower yield for the 250 eV point.

For engineering calculations, the erosion rate is often a more meaningful way to present comparisons of sputtering data since one does not have to correct for differing material densities to assess relative performance. The erosion rate is related to the sputter yield by the following relation;

$$\dot{R} = \frac{h_{eff}}{\tau} = \left(\frac{M}{e \rho N_{AVO}} \right) Y \bar{j} \tag{8}$$

where $\bar{j}$ is the mean current density (including energetic neutrals) averaged over the duration of the exposure. This can be determined from the previous expression (Equation 4) for the dosage of energetic particles by

$$\bar{j} = \frac{e}{\tau} N_E = \frac{1}{\tau} \left(Q_b^+ + \frac{1}{2} Q_b^{++} + \int_0^\tau J_n(t) dt \right) \tag{9}$$

The erosion rate results for the three materials are presented in Figure 5 with values normalized to a current density of 1 mA/cm^2. Although carbon-carbon and diamond have the same molecular weight, the density of diamond is higher. As evident from Equation 7, the yield is proportional to the product of

the eroded depth and the density. For this reason the yield of diamond is higher than carbon-carbon while its erosion rate, which is independent of density, is lower.

The sputter yields of single crystal solids is known to be dependent on both the crystallographic plane and its orientation relative to the incident beam[24]. Interpretation of the yield data vs. energy for the single crystal diamond was complicated by the fact the sample used for the 500 eV was found to have a (100) plane exposed to the beam as opposed to the other samples which had a (110) plane exposed. The incidence angle can have a much more pronounced effect on the yield of single crystal materials as compared with polycrystalline. This is due in part to channeling effects in which incident ions can penetrate more deeply into the target when the beam is aligned with specific lattice directions. Energy deposition at these deeper layers usually result in lower sputter removal of material and appear as a series of dips superimposed on the $\cos^{-1}$ yield versus incidence angle curve. Whetten et al. measured sputter yields of (100) single crystal diamond subject to argon ion bombardment at 500 eV as a function of incidence angle[5]. The measured values ranged from approximately 0.14 at normal incidence to 0.28 at an angle of 25 degrees. The values measured here for xenon at the same energy was nominally 0.06 at an incidence angle of approximately 15 degrees.

Examination of the surface topography of the single crystal diamond samples after exposure to the ion beam revealed fairly uniform pitting of the surfaces for incident ion energies of 500 eV and lower. Figure 6a is representative of this structure. The eroded surface of the crystal exposed to 750 eV ions showed no pitting even at magnification of 50,000 X. This sample showed evidence of transformation of the crystal structure into "terrace" formations as shown in Figure 6b. Other groups have reported and proposed explanations for damage induced structural transformation of (110) single crystal diamond surfaces subject to argon ion irradiation at 1 keV[10], and polycrystalline diamond subject to neon ion irradiation at 0.1 - 1.6 keV[11]. It is possible the observed structures are evidence of such transformations as well.

Conclusions

Sputter yields were measured for molybdenum, carbon-carbon, single crystal, and polycrystalline diamond subject to xenon ion bombardment in the energy range of 150 to 750 eV. The experimental approach used introduces a number of potential effects which can influence the calculated yields. Two significant sources of uncertainty in the evaluation of the yields stem from charge-exchange processes which produce thermal ions and energetic neutrals, and the effects of non-normal incidence. In terms of application of diamond film coatings as a way of increasing lifetime for ion thruster electrodes subject to sputter erosion, CVD diamond films should provide at least a factor 10 improvement in erosion rate over molybdenum and 1.5 over carbon-carbon. Finally, examination of surface topography for the single crystal diamond revealed evidence of crystalline transformation at incident ion energy of 750 eV.

Acknowledgments

The work described in this paper was performed by the Jet Propulsion Laboratory (JPL), California Institute of Technology, under contract with the National Aeronautics and Space Administration. The authors wish to express their thanks to Prof. M. Nicolet at Caltech for use of the Sputter Deposition Laboratory, Dr. R. Koba of Crystalline Materials Corp. for providing the CVD diamond sample used in this work, and Drs. J. Brophy and J. Wang of JPL for assistance with analysis of the ion source and plume.

References

1. Davis, R.F., Ed., Diamond Films and Coatings; Development, Properties, and Applications, Noyes Publications, Park Ridge, NJ, 1993.

2. Zhu, W., Stoner, B.R., Williams, B.E., and Glass, J.T., "Growth and Characterization of Diamond Films on Non-diamond Substrates for Electronic Applications", Proceedings of the IEEE, **79**(5), May 1991, pp. 621-646.

3. Ashfold, M. N., May, P.W., Rego, C.A., and Everitt, N.M., "Thin Film Diamond by Chemical Vapour Deposition Methods", Chemical Society reviews, 1994, pp. 21-30.

4. Blandino, J. J., Goodwin, D.G., Garner, C.E., Brophy, J.R., "Evaluation and Development of Diamond Grids for Ion Optics", AIAA 95-2663, Presented at the 31st Joint Propulsion Conference, July 10-12 1995 San Diego, CA.

5. Whetten, T. J., Armstead, A., A., Grzybowski, T., A., Ruoff, A.,L., "Etching of Diamond with Argon and Oxygen Ion Beams", J.Vac.Sci. Tech. A, Vol. April-June, 1984, pp. 477.

6. Miyamoto, I.,and Taniguchi, N., "Polishing and Sharpening of Diamond Point Tools by Ion Sputter-Machining", Precision Engineering, **4**, No 4, Oct. 1982, pp. 191.

7. Hirata, A., Tokura, H., Yoshikawa, M., "Smoothing of Chemically Vapor Deposited Diamond Films by Ion Beam Irradiation", Thin Solid Films, 212, 1992, pp. 43-48.

8. Kobayashi, K., Yamamoto, K., Mutsukura, N., Machi, Y., "Sputtering Characteristics of Diamond and Hydrogenated Amorphous Carbon Films by R.F. Plasma", Thin Solid Films, 185, 1990, pp. 71-78.

9. Ullmann, J., Delan, A., Schmidt, G., "Ion Etching Behavior and Surface Binding Energies of Hard Diamond-Like Carbon and Microwave Chemical Deposition Diamond Films", Diamond and Related Materials, **2**, 1993, pp. 266-271.

10. Hoffman, A., Prawer, S., Kalish, R., "Structural Transformation of Diamond Induced by 1-keV Ar-ion Irradiation as Studied by Auger and Secondary-Electron Spectroscopies and Total-Secondary-Electron-Yield Measurements", Physical Review B, **45**(22), June 1992, pp. 736 - 745.

11. Ullmann, J., Weber, A., Mainz, B., Stiegler, J., and Schuhrke, T., "Low Energy Ion-Induced Damage of Polycrystalline Diamond Films", Diamond and Related Materials, **3**, 1994, pp. 663-671.

12. Joshi, A., Nimmagadda, R., "Erosion of Diamond Films and Graphite in Oxygen Plasma", J. Material Res. **6**, No 7, July 1991, pp. 1484.

13. Dorsch, O., Werner, M., and Obermeier, E., "Dry Etching of Undoped and Boron Doped Polycrystalline Diamond Films", Diamond and Related Materials, **4**, 1995, pp. 456-459.

14. Sandhu, G.S., and Chu, W.K., "Reactive Ion Etching of Diamond", Applied Physics Letters, **55**(5), 1989, pp. 437-438.

15. Efremow, N.N., Geis, M.W., Flanders, D.C., Lincoln, G.A., and Economou, N.P., "Ion Beam Assisted Etching of Diamond", J. of Vac. Sci. Technol. B **3**(1), Jan/Feb 1985, pp. 416-418.

16. Garner, C.E., Brophy, J.R., Pless, L.C., and Barnett, J.W. "The Effect of Nitrogen on Xenon Ion Engine Erosion", AIAA 90-2591, Presented at the 21st International Electric Propulsion Conference, July 18-20, 1990 Orlando, FL.

17. Hagstrum, H.D., "Effect of Monolayer Adsorption on the Ejection of Electrons from Metals by Ions", Physical Review, **104**(6), 1956, pp. 1516-1527.

18. Kim, J. K., Kheyrandish, H., and Colligon, J.S., "Influence of Charge Exchange on Ion/Neutral Arrival Rates in an Ion-Assisted Deposition System", J. Vac. Sci. Technology A, V12, No 5, Sept.-Oct. 1994, pp. 2733-2738.

19. Samanta Roy, R.,"Numerical Simulation of Ion Thruster Plume Backflow for Spacecraft Contamination Assessment", Ph.D. Dissertation, Dept. of Aeronautics and Astronautics, MIT, June 1995.

20. Rosenberg, D. and Wehner, G.K. ,"Sputtering Yields for Low Energy He, Kr, and Xe Ion Bombardment", J. App. Phys. **33**(5), 1962, pp. 1842 - 1845.

21. Weijsenfeld, C.H., Hoogendoorn, A., and Koedam, M. "Sputtering of Polycrystalline Metals by Inert Gas Ions of Low Energy (100 - 1000 eV)", Physica, **27**, 1961, pp. 763-764.

22. Wehner, G. "Influence of the Angle of Incidence on Sputtering Yields", J. App. Phys. **30**(11), 1959, pp. 1762 - 1765.

23. Mueller, J., Brophy, J.R., and Brown D.K., "Endurance Testing and Fabrication of Advanced 15-cm and 30-cm Carbon-Carbon Composite Grids", AIAA 95-2660, Presented at the 31st Joint Propulsion Conference, July 10-12 1995 San Diego, CA.

24. Behrisch, R. , Ed. Sputtering by Particle Bombardment I; Physical Sputtering of Single-Element Solids, Springer-Verlag Berlin Heidelberg, 1981, pp. 200-203, 219-222.

Table 1. Base and test pressures, average current densities at the target, and the time averaged incidence angles. Uncertainty in incidence angles can be approximated by the beam divergence to be (+/-) 5-10 degrees.

Energy	Base Press.	Test Press.	J_{ave} Moly, C-C, CVDDia	J_{ave} Sing Cryst Dia	Incidence Angle
(eV)	(Torr x 10^{9})	(Torr x 10^{4})	(mA/cm^2)	(mA/cm^2)	(deg)
150	7.7	2.1	0.75 +/- 0.08	0.74 +/- 0.08	12
250	1.1	2.1	1.66 +/- 0.14	1.64 +/- 0.14	12
500	11.0	2.1	3.59+/- 0.77	3.46 +/- 0.81	15
750	2.3	2.1	5.22 +/- 1.12	5.03 +/- 1.18	9

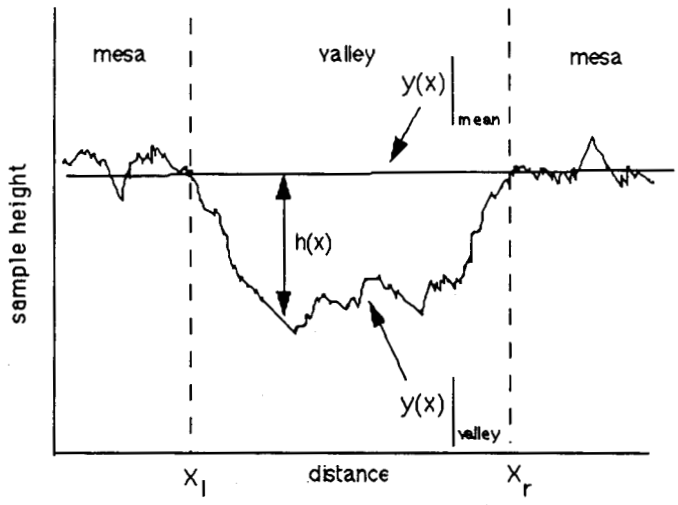

Figure. 1. Schematic of profilometer trace illustrating mesa curve fit which defines datum for depth measurements.

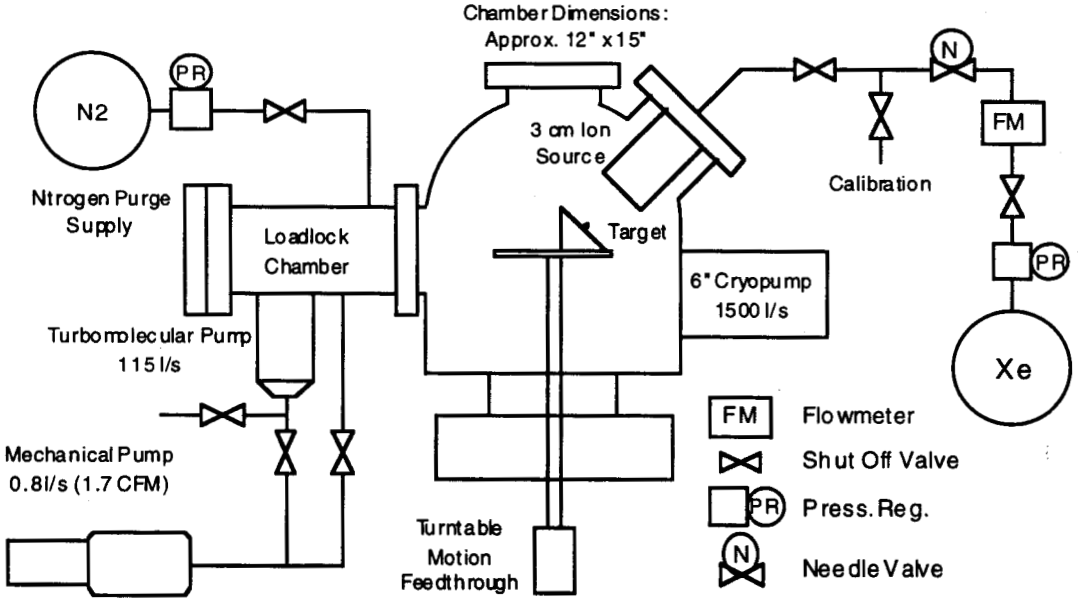

Figure 2. Schematic of the Ultra-High-Vacuum test system

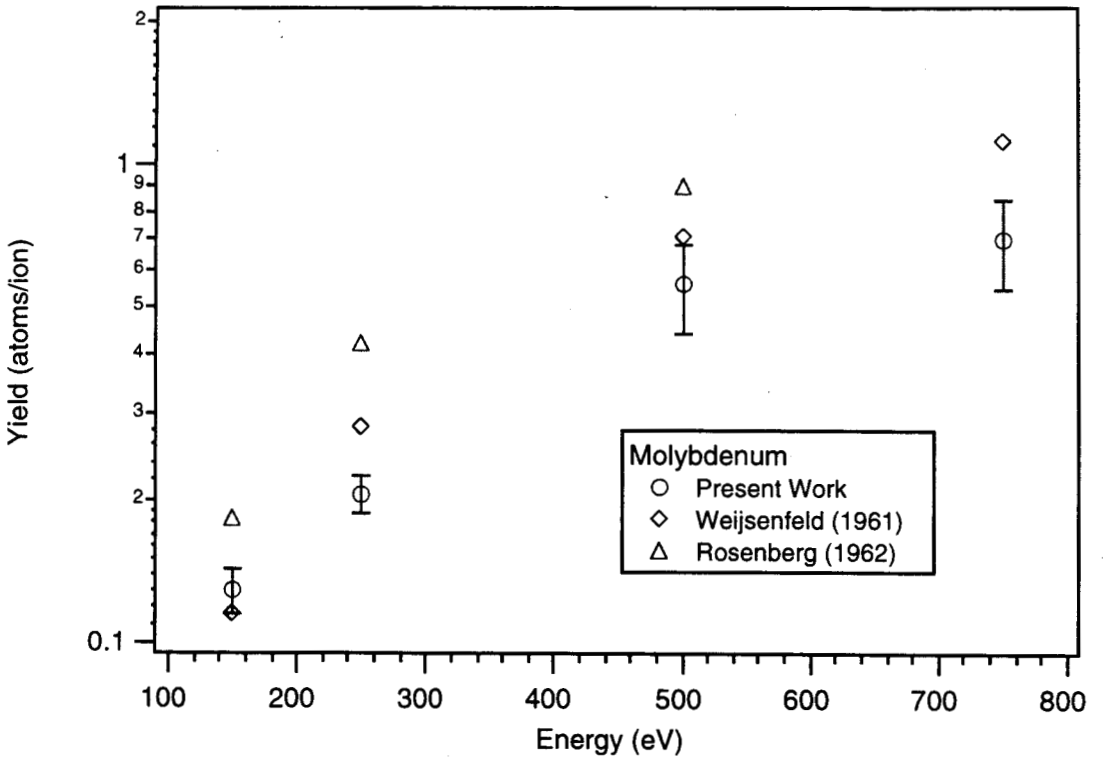

Figure. 3. Comparison of molybdenum yield with data of Weijsenfeld and Rosenberg.

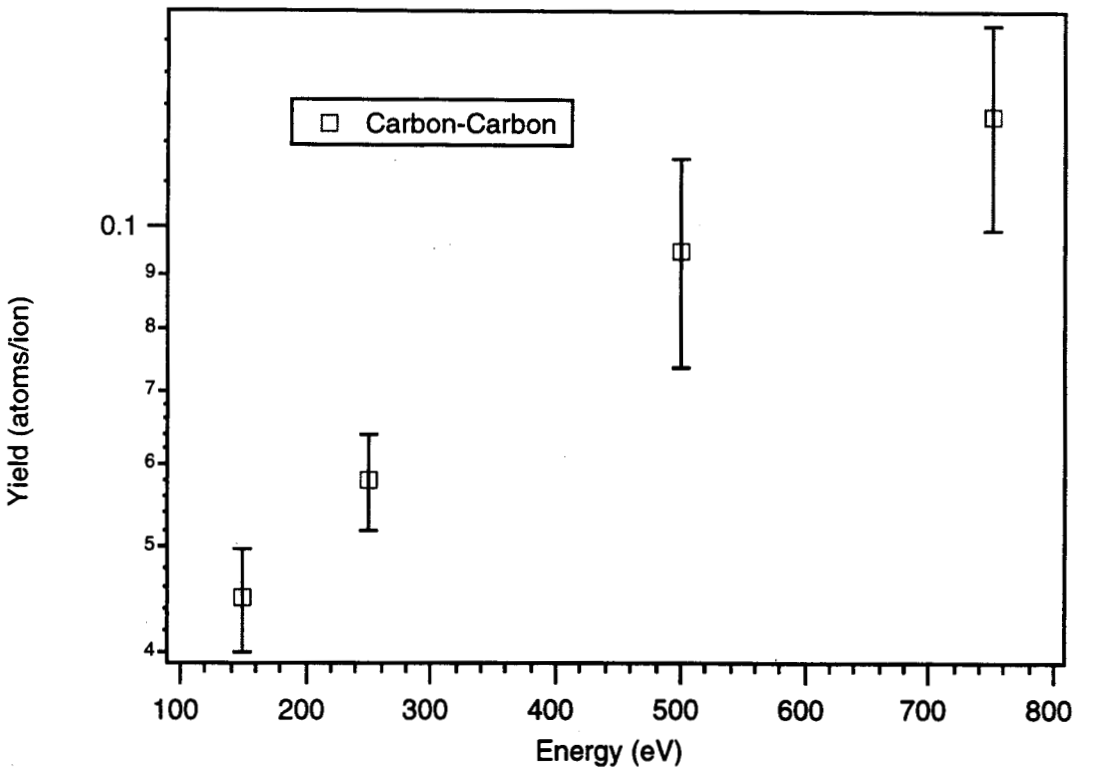

Figure. 4a. Sputter yields for carbon-carbon composite

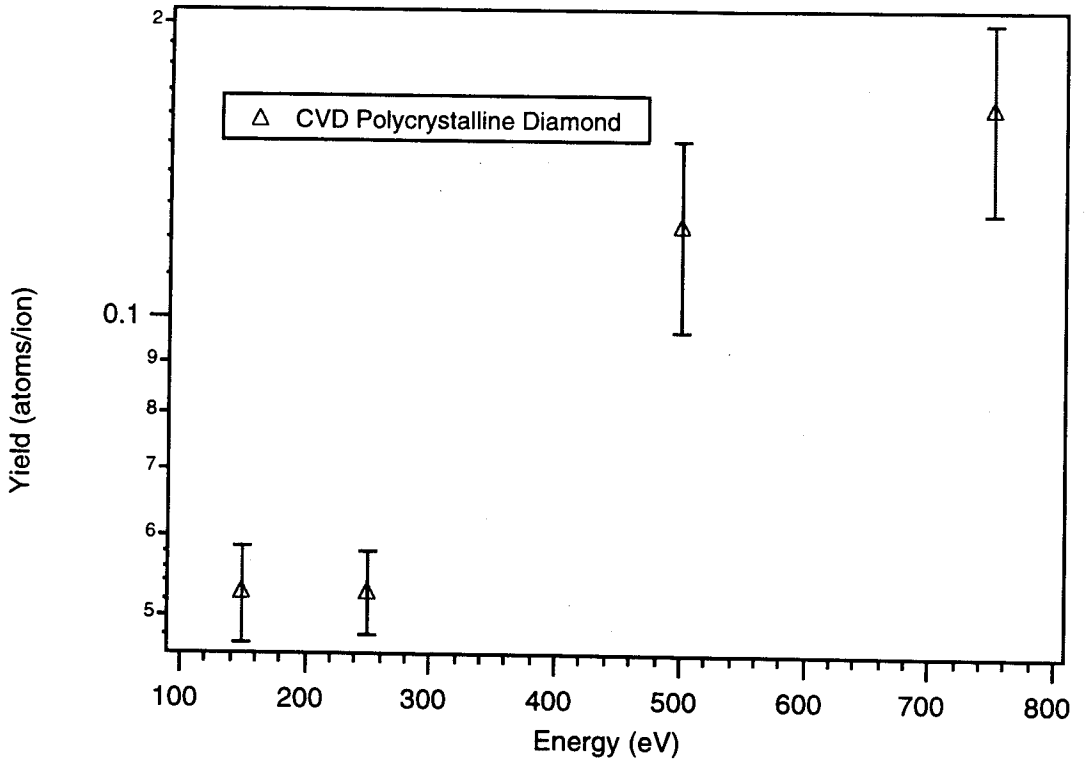

Figure. 4b. Sputter yields for polycrystalline CVD diamond

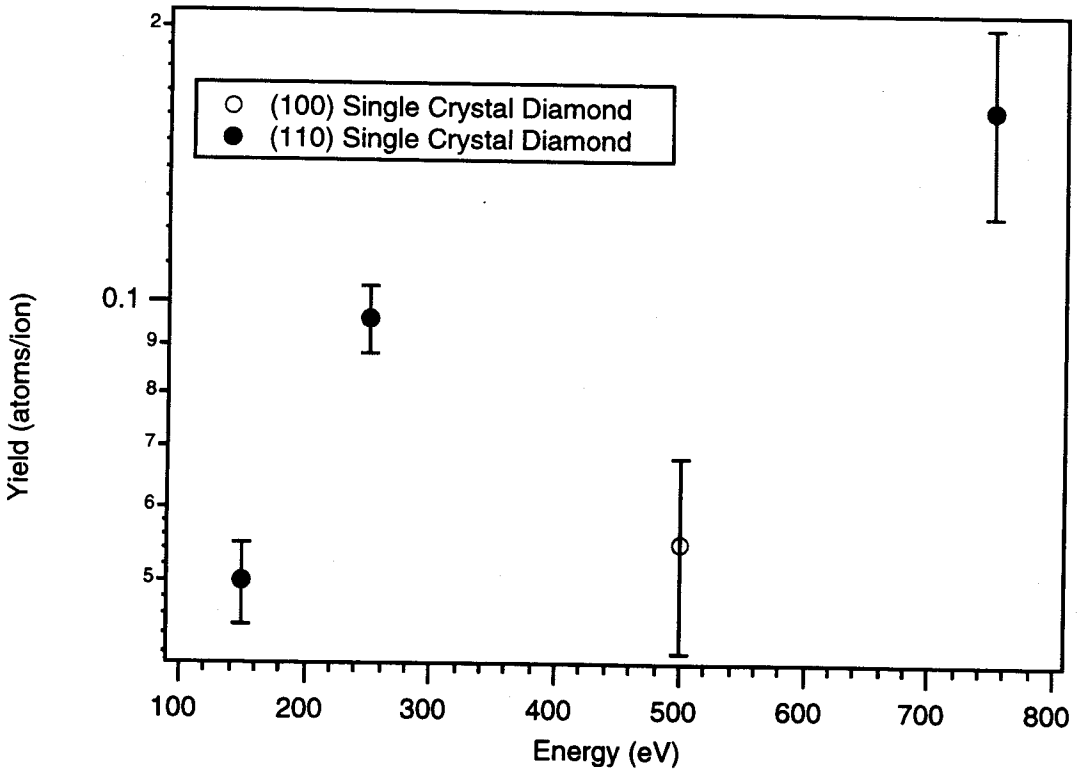

Figure. 4c. Sputter yields for single crystal diamond

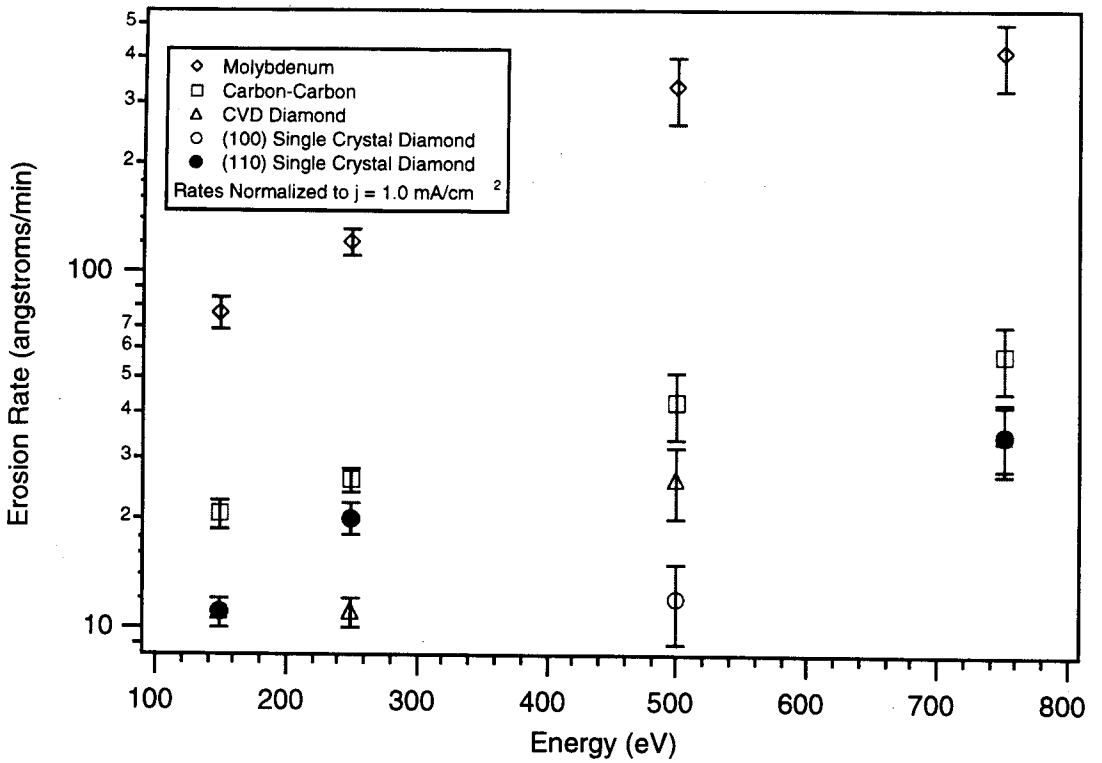

Figure. 5. Erosion rates normalized to incident current density of 1 mA/cm^2.

Figure. 6. SEM Images of single crystal diamond after sputtering. a) 5000 x Mag of (100) surface exposed to 500 eV ions showing fine pitting, b) 4000 x Mag of (110) surface exposed to 750 eV ions. "Terrace" like features suggest transformation of crystalline structure.

6a)

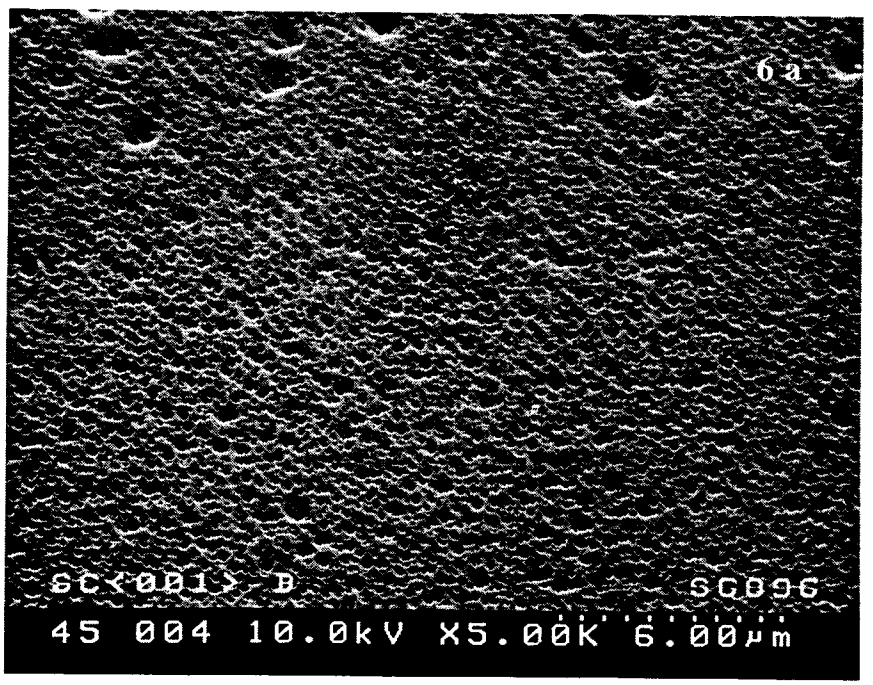

6b)